Hybrid Imaging Kernel Calibration Applied on Microwave Scanner for Brain Stroke Monitoring

C. Origlia, D. O. Rodriguez-Duarte, J. A. Tobon Vasquez, F. Vipiana
Dept. Electr. and Telecommunications, Politecnico di Torino, Torino, Italy
Email: francesca.vipiana@polito.it

***Abstract*—This paper validates a calibration procedure applied on a microwave imaging (MWI) kernel based on the combination of pre-computed simulated data and available S-parameters measurements. The assessed technique compensates for the image degradation caused by mild and non-modeled features of the imaging device, such as the unavoidable manufacturing discrepancies in the antenna array. The testing considers a synthetically mimicked experimental scenario of a hemorrhagic stroke condition and a realistic scanner prototype. This approach allows a thorough comparative assessment of the calibration effect on the electric field estimation used by the MWI algorithm, hardly achievable with measurements. The results show the capability of the calibration procedure to reduce the retrieved images' distortions and artifacts compared to the non-calibrated approach, being an essential milestone toward its application in real-life scenarios.**

***Index Terms*—Measurements calibration, microwave imaging, numerical simulation, microwave antenna arrays, microwave propagation.**

I. INTRODUCTION

Brain stroke is a hazardous pathological condition that occurs when an artery to the brain clots or bursts, provoking post-onset disability or death, and requiring prompt medical intervention. In this context, microwave imaging (MWI) technology is an on-development imaging-based alternative for diagnosis and follow-up that presents advantages in terms of time examination, safety, and portability, albeit limited spatial resolution [1]. MWI relies on the electric contrast between the healthy tissues and the damaged area at microwave frequencies for retrieving quantitative or qualitative maps of the region of interest from a limited number of measurements. It is, thus, a nonlinear and ill-posed inverse scattering problem, which might cause corrupted images with unwanted artifacts if it is either not well-conditioned or inappropriately modeled.

To make the imaging inversion mechanism more robust and improve the outcomes, calibration techniques are applied, aiming to match the experimental system and the nominal modeled one used for building the imaging kernel, as well as mitigating multiplicative inaccuracies.

Traditional calibration procedures use measured S-parameters of *known* scenarios to get the calibration coefficients to be applied to the *unknown* experimental data [2]–[6]. However, depending on the application, the use of a known target is unfeasible or inconvenient. Thus, novel alternatives have been proposed in the literature, as in [7], where a single measured dataset in the unknown state is first used to obtain a parametric calibration model, than pre-channel calibration coefficients are obtained to calibrate the unknown fields.

In this manuscript, we assess a complementary and innovative calibration framework that potentially compensates for variables of different natures, from physical inaccuracies in the probes, to the external electronics phase shifts. Unlike other techniques that work on the S-parameters, our proposed method consists of adjusting the electric field used to build the imaging kernel (i.e. the operator) relying on a single measured S-parameters set and an offline computed synthetic dataset, which is made via parametric full-wave numerical simulations. Specifically, it is considered a realistic simulated scenario using the MWI system presented in [8] and illustrated in Fig. 1, and a mimicked intracranial hemorrhagic stroke condition.

II. METHODS

A. Calibration Framework

MWI algorithms require to build an imaging kernel based on the electric field (E) in a reference scenario. It is usually computed via high-fidelity full-wave electromagnetic simulation, exploiting a-priori information about the studied case. However, a mismatch between the digital model and the actual

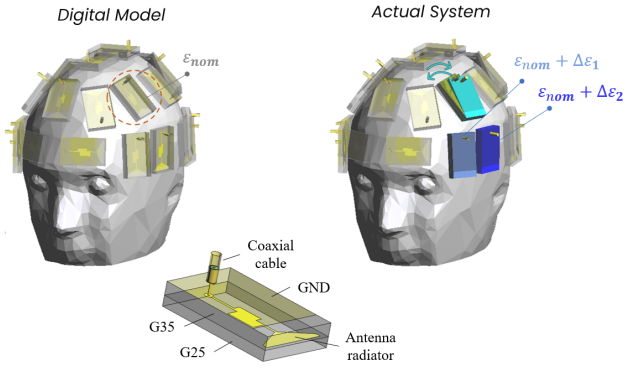

Fig. 1. Diagram of the MWI device for brain stroke monitoring. (Left): nominal system; (middle) brick antenna model [8]; (right): representation of a realistic system with positioning errors and tolerances of the antennas dielectric properties with respect to the nominal value, ϵ_{nom}.

This work was supported by the Italian Ministry of University and Research under the PRIN project "MiBraScan", and by the European Union's Horizon 2020 Research and Innovation Program under the EMERALD project, Marie Sklodowska-Curie grant agreement No. 764479.

system always arises because of measurements uncertainty and modeling errors, e.g. those resulting from manufacturing tolerances and positioning errors in the antenna array, or phase shifts and signal distortion due to the electrical path feeding the probes (see Fig. 1).

The calibration proposed aims to mitigate the variations between the nominal numerical model and the real device. Thus, it is intended to improve the reliability of the imaging operator, and finally enhance the accuracy of the output image. The procedure is developed in three main steps:

1) A *learning* step creates a simulated dataset of S-parameters and E, representing the expected variations of the physical system. It provides a set of N orthogonal basis functions, $[\Psi]$, such that the real measured data, $[S^{\mathrm{m}}]$, can be written through the following linear combination:
$$[S^{\mathrm{m}}] \cong \sum_{n=1}^{N} \alpha_n \Psi_n, \tag{1}$$
where $[\alpha]$ are the calibration coefficients.
2) A single *S-parameters measurement* is collected and projected on the previously build basis. The calibration coefficients are computed so that the numerical scenario matches the real one:
$$[\alpha] = [\Psi]^{\dagger}[S^{\mathrm{m}}], \tag{2}$$
3) By last, the calibrated E is obtained as a linear combination of the simulated E, through the calibration coefficients, $[\alpha]$.

A more detailed description of the mathematical background of the technique is found in [9]. Notice that, although the first step requires high computational effort, it is performed *offline*, i.e., separately from the measurements, implying that the method is still feasible for real-time MWI applications.

B. Synthetic Setup

Here, we preliminary validate the calibration method in a simulated scenario, exploiting an in-house full-wave EM solver based on the finite element method (FEM) [10]. This approach provides a controlled experiment where the investigated variables can be dynamically selected and the effects on the resulting E directly evaluated.

As aforementioned, we applied the calibration scheme to the system presented in [8], consisting of 22 custom monopole antennas, working around 1 GHz. Then, following the steps described in the previous section, we first build a synthetic dataset by parametrically varying the dielectric properties of the matching medium and the dielectric brick of the antennas. Indeed, these materials are made of custom mixtures of urethane rubber and graphite powder (referred to as G25 and G35, respectively, in Fig. 1), subject to manufacturing inaccuracies that result in variations in the antenna response [9].

Aiming to numerically emulating the real-life measurement setup, we realized a *target scenario* as a perturbed digital model. To this end, the model was altered by considerably shifting the selected variables. It is worth noticing that, to ensure the meaningfulness of the validation, the target scenario is not included in the calibration synthetic model, mimicking the uncertainty of the measurements. This procedure provides us with the ideal E, which is the target for the calibrated E.

Afterward, the E are used to compute the imaging operators as follows:

- the *nominal* operator considers all the antennas are identical, which is the traditional approach for building the imaging kernel;
- the *ideal* operator, which gives the best performance in the target scenario;
- the *calibrated* operator;

Their performance are compared for a simulated case of hemorrhagic brain stroke, simplified as a spherical region having blood's properties, located in the central back part of the brain. Here, we consider a well-assessed imaging inversion method called truncated singular value decomposition (TSVD), taking in input the differential S-parameters at two time instants: t_0, which corresponds to the "healthy" situation, and t_1, when the stroke appears. Moreover, the algorithm exploits the distorted Born approximation; more details can be found in [8]. In the specific, here, the imaging is obtained with a single frequency approach, though both the imaging algorithm and the calibration scheme can work with multi-frequency data.

III. RESULTS

We split the results into two consecutive parts to validate the calibration scheme under the actual imaging task. The objective is to assess the effects caused by the non-modeled variations on the building of the imaging kernel. Hence, we evaluate the extent of the propagation of the modeling errors and calibration benefits in the imaging retrieval.

First, we compare the nominal, ideal, and calibrated fields. The ideal one is the actual field of the realistic target system, where the antennas have uncontrolled complex permittivity variation with respect to the nominal one. We denominated it as ideal since it is the best possible field to build the kernel. It is worth noticing here that obtaining the field of real-life experimental validation scenarios is not trivial, giving more value to the calibration assessment using synthetic tests.

Considering the final aim of the calibration is to make the MWI more robust, the second part of the results examines the effect of selecting the nominal, ideal, and calibrated field for building the imaging kernel and then the retrieved images. Hence, the imaging algorithm receives as input the set of target S-parameters and applies it to the three studied kernels.

A. Electric Fields Reconstruction

To illustrate the differences between the considered cases, we select a transverse slide of the complete 3-D distribution while one of the antennas is active, though, the variation in the field is distributed over the whole domain. Figure 2 depicts the three situations, where on top is reported the magnitude of the field and at the bottom the phase.

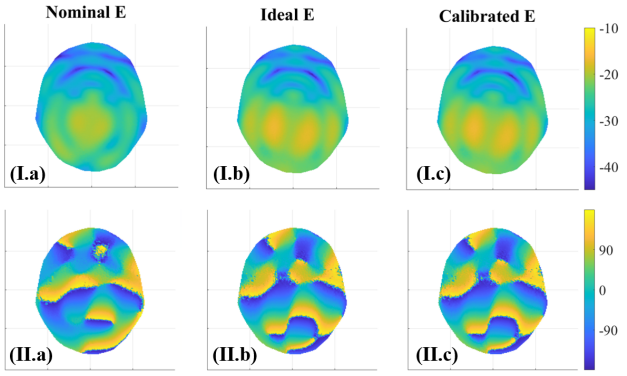

Fig. 2. Transversal view of the electric field distribution cut at the middle of the head. (Top): $|E|$ [dBμV/m^2]; (Bottom): $\varnothing(E_x)$[deg].

Using the specific field sample as a reference, we can first notice the discrepancies in magnitude and phase between the nominal and the ideal case and, second, the positive effect of the calibration. The former demonstrates how the limited modeling of the actual system introduces errors directly in the kernel building, which thus propagate to the imaging generation. The latter shows the calibration compensation of the field distortions, providing a more proper approximation of the ideal field.

B. Imaging Evaluation

This part of the results evaluates the effects of the different projected imaging kernels directly on the imaging. Then, the testing retrieves the dielectric contrast maps of a simplified hemorrhagic stroke condition using the prototype under calibration. Hence, aligned with the previous results, here we present the retrieved images using each of the operators as shown in Fig. 3, from left to right, respectively.

On the left, the nominal case represents the worst and standard scenario. As expected, its response is degraded with the increase of artifacts and, most importantly, the distortion of the estimated stroke target. Though this degradation seems inconsequential, in a real-life system it will be scaled and worsted by introducing multiple additional and non-calibrated sources of errors, such as slight deviations in the positioning of the antennas. The best case is illustrated in the middle, showing the target's faithful and clean reconstruction. Finally, on the right, the retrieved contrast demonstrates an improvement in the quality and agreement with the ideal case.

IV. CONCLUSIONS

In this paper, we present a complete synthetic evaluation of a hybrid calibration technique that compensates for non-modeled features. It acts on the electric field used to build the imaging operator of MWI systems, here a scanner for brain stroke monitoring. The problem was narrowed by simplifying the mimicked clinical condition, limiting the sources of non-modeled errors to bound, and focusing on evaluating the technique in a more controlled methodology. The results then

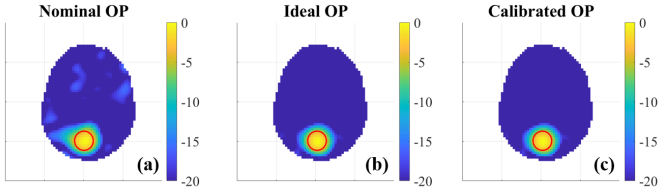

Fig. 3. Transverse view of the normalized amplitude values of the reconstructed dielectric contrast in [dB]; cut in their maximum. The red circle indicates the stroke contour. OP stands for operator.

show a great potential to solve the problems caused by the non-modeling of features that are adequately included in the calibration basis. Synthetic assessment is a pivotal step in studying the method. Notice also that the calibration technique does not depend on the device or the imaging algorithm, thus can be applied to other systems. In the future, we plan to extend the evaluation to real-life conditions exploiting its real-time nature and completing the basis with additional variables.

REFERENCES

[1] A. Kiourti, A. M. Abbosh, M. Athanasiou, T. Björninen, A. Eid, C. Furse, K. Ito, G. Lazzi, M. Manoufali, M. Pastorino, M. M. Tentzeris, K. Tisdale, E. Topsakal, L. Ukkonen, W. G. Whittow, H. Zhang, and K. S. Nikita, "Next-generation healthcare: Enabling technologies for emerging bioelectromagnetics applications," *IEEE Open Journal of Antennas and Propagation*, vol. 3, pp. 363–390, 2022.

[2] M. Ostadrahimi, P. Mojabi, C. Gilmore, A. Zakaria, S. Noghanian, S. Pistorius, and J. LoVetri, "Analysis of incident field modeling and incident/scattered field calibration techniques in microwave tomography," *IEEE Antennas and Wireless Propagation Letters*, vol. 10, pp. 900–903, 2011.

[3] S. Tu, J. McCombe, D. Shumakov, and N. Nikolova, "Fast quantitative microwave imaging with resolvent kernel extracted from measurements," *Inverse Problems*, vol. 31, no. 4, 2015.

[4] D. O. Rodriguez-Duarte, J. A. Tobon Vasquez, R. Scapaticci, G. Turvani, M. Cavagnaro, M. R. Casu, L. Crocco, and F. Vipiana, "Experimental validation of a microwave system for brain stroke 3-d imaging," *Diagnostics*, vol. 11, no. 7, 2021.

[5] T. M. Grzegorczyk, P. M. Meaney, P. A. Kaufman, R. M. diFlorio Alexander, and K. D. Paulsen, "Fast 3-d tomographic microwave imaging for breast cancer detection," *IEEE transactions on medical imaging*, vol. 31, p. 1584—1592, August 2012.

[6] L. Guo, N. Nguyen-Trong, A. AI-Saffar, A. Stancombe, K. Bialkowski, and A. Abbosh, "Calibrated frequency-division distorted born iterative tomography for real-life head imaging," *IEEE Transactions on Medical Imaging*, vol. 41, no. 5, pp. 1087–1103, 2022.

[7] E. Kim, C. T. Mohammadi, M. Asefi, J. Lovetri, I. Jeffrey, and C. Gilmore, "Imaging and calibration of electromagnetic inversion data with a single data set," *IEEE Open Journal of Antennas and Propagation*, vol. 3, pp. 12–23, 2022.

[8] D. O. Rodriguez-Duarte, C. Origlia, J. A. T. Vasquez, R. Scapaticci, L. Crocco, and F. Vipiana, "Experimental assessment of real-time brain stroke monitoring via a microwave imaging scanner," *IEEE Open Journal of Antennas and Propagation*, vol. 3, pp. 824–835, 2022.

[9] D. O. Rodriguez-Duarte, J. A. Tobon Vasquez, and F. Vipiana, "Hybrid simulation-measurement calibration technique for microwave imaging systems," in *2021 15th European Conference on Antennas and Propagation (EuCAP)*, pp. 1–5, 2021.

[10] D. O. Rodriguez-Duarte, J. A. T. Vasquez, R. Scapaticci, L. Crocco, and F. Vipiana, "Assessing a microwave imaging system for brain stroke monitoring via high fidelity numerical modelling," *IEEE Journal of Electromagnetics, RF and Microwaves in Medicine and Biology*, vol. 5, no. 3, pp. 238–245, 2021.